Submillimeter Accuracy of InSAR Time Series: Experimental Validation

Alessandro Ferretti, *Member, IEEE*, Giuliano Savio, Riccardo Barzaghi, Alessandra Borghi, Sergio Musazzi, Fabrizio Novali, Claudio Prati, and Fabio Rocca

***Abstract*—This paper presents the results of a blind experiment that is performed using two pairs of dihedral reflectors. The aim of the experiment was to demonstrate that interferometric synthetic aperture radar (InSAR) measurements can indeed allow a displacement time series estimation with submillimeter accuracy (both in horizontal and vertical directions), provided that the data are properly processed and the impact of *in situ* as well as atmospheric effects is minimized. One pair of dihedral reflectors was moved a few millimeters between SAR acquisitions, in the vertical and east–west (EW) directions, and the ground truth was compared with the InSAR data. The experiment was designed to allow a multiplatform and multigeometry analysis, i.e., each reflector was carefully pointed in order to be visible in both Envisat and Radarsat acquisitions. Moreover, two pairs of reflectors were used to allow the combination of data gathered along ascending and descending orbits. The standard deviation of the error is 0.75 mm in the vertical direction and 0.58 mm in the horizontal (EW) direction. GPS data were also collected during this experiment in order to cross-check the SAR results.**

***Index Terms*—Artificial reflector, global positioning system (GPS), interferometric synthetic aperture radar (InSAR), permanent scatterer (PS).**

I. Introduction

As well known, temporal and geometric decorrelation represents the most important limiting factor in synthetic aperture radar interferometry (InSAR) [1]. Due to this fact, analyses of low coherence areas (e.g., forested and vegetated areas) with conventional InSAR methodologies cannot be performed successfully. Even the application of advanced InSAR algorithms, such as the permanent scatterer (PS) technique [2], may prove to be ineffective wherever the density of stable radar targets (i.e., the PS) is extremely low.

In order to overcome this limitation, the usage of artificial reflectors can be very promising. Basically, an artificial reflector is an object that exhibits a high radar cross section (RCS)—or, at least, a good signal-to-clutter ratio (SCR)—stable in time. This feature allows one to carry out the interferometric measurements with a high signal-to-noise ratio (SNR).

Apart from their deployment in low coherence areas to create measurement points, artificial reflectors have already been used in previous works to assess the accuracy of the InSAR measurements [3]–[7]. However, usually, the experiment focused on the detection and/or the measurement of just one component of the displacement vector affecting the phase center of an artificial radar target, typically a corner reflector. In fact, since InSAR data measure range variations (i.e., the component of the displacement vector along the satellite line of sight—LOS), the full 3-D displacement vector can be recovered using three or more independent InSAR datasets corresponding to noncoplanar acquisition geometries, unless additional assumptions on the motion can be exploited. To the authors' knowledge, so far, a blind experiment to assess the accuracy of both vertical and horizontal components of the displacement vector using two acquisition geometries has not been performed yet.

In this paper, we will discuss the results achieved in a new field test with artificial reflectors. The main goal of this project was to demonstrate that the InSAR data can indeed allow the measurement of displacement time series with submillimeter accuracy (both in horizontal and vertical directions) once the radar acquisitions are properly processed and the impact of *in situ* as well as atmospheric effects is minimized. As an additional result, the possibility of using properly oriented dihedral reflectors to create high RCS targets in urban areas for two different satellite radar sensors, characterized by different orbits and antenna squint angles, was confirmed. Preliminary results were presented during the ESA-FRINGE Workshop by Frascati [8]. Here, all SAR data have been reprocessed, achieving better results.

Although not specifically designed for GPS-InSAR comparison, the experimental setup was used to measure the vertical displacement of the mobile reflectors using two GPS antennas, creating another dataset to cross-check the results.

This paper is organized as follows: first, the design phase of the experiment is briefly summarized in Section II. Then, a description of the technical and mechanical details of the artificial reflectors is reported (Section III). The subsequent section presents the deployment procedure and how the test area was identified based on amplitude data (Section IV). In Section V, the experimental results are reported, while in Sections VI and VII, the results are discussed and conclusions are drawn.

II. Experimental Setup

In order to assess the accuracy of satellite InSAR measurements in both vertical and horizontal directions, an experiment involving two pairs of artificial reflectors has been set up. Each pair of reflectors is composed of two radar targets mounted on a

Manuscript received July 18, 2006; revised November 28, 2006. This work was supported by the public fund for the Italian Electric System.

A. Ferretti, G. Savio, and F. Novali are with the Tele-Rilevamento Europa, 20149 Milan, Italy (e-mail: giuliano.savio@treuropa.com).

R. Barzaghi and A. Borghi are with the DIIAR, Politecnico di Milano, 20133 Milan, Italy.

S. Musazzi is with the CESI Ricerca, 20134 Milan, Italy.

C. Prati and F. Rocca are with the Dipartimento di Elettronica ed Informazione, Politecnico di Milano, 20133 Milan, Italy.

Digital Object Identifier 10.1109/TGRS.2007.894440

TABLE I
RCSs OF THE MOST COMMON ARTIFICIAL REFLECTORS

ARTIFICIAL REFLECTOR	MAX RCS [m^2]	Example: C-band (λ=5.66 cm)	NUMBER OF SENSORS THAT CAN BE USED
Rectangular Flat Plate	$\frac{4\pi a^2 b^2}{\lambda^2}$	a = b = 1 m $\rightarrow$ RCS = 3922 m^2	1
Rectangular Dihedral	$\frac{8\pi a^2 b^2}{\lambda^2}$	a = b = 1 m $\rightarrow$ RCS = 7845 m^2	2
Triangular Trihedral	$\frac{4\pi a^4}{3\lambda^2}$	a = 1 m $\rightarrow$ RCS = 1375 m^2	> 2
Square Trihedral	$\frac{12\pi a^4}{\lambda^2}$	a = 1 m $\rightarrow$ RCS = 11768 m^2	> 2

common metallic basement: one is visible along ascending orbits of the satellite and the other one is visible along descending orbits. One pair is fixed and used as a reference point. The other pair is installed on a platform that can be shifted horizontally and vertically with submillimetric accuracy.

In principle, the use of four independent datasets acquired by two different sensors (i.e., Envisat and Radarsat) along ascending and descending orbits would allow the recovery of the full 3-D displacement vector affecting the radar target. However, due to the limited number of scenes that could be acquired during the duration of the experiment (about ten months) and the unfavorable SNR achievable in the north–south direction [9], [10], it was decided to limit the displacement of the moving reflectors to the east–west (EW) and vertical components only.

The type of artificial reflector to be used in the experiment was designed to maximize the RCS and the SCR of the target to allow accurate phase measurements while keeping the weight and the overall dimensions as small as possible. The latter constraints are required to guarantee a high mechanical stability and a positioning accuracy of the mobile reflectors better than 1 mm. Moreover, the selected reflectors had to be visible in both Envisat and Radarsat acquisitions, both platforms having radar sensors operating at C-band.

As far as the first point is concerned, the reflector should be characterized by a reflectivity much higher than the surrounding scatterers. In fact, the reflector has to be easy to identify in the radar image, and its SCR, i.e., the ratio between the RCS of the reflector and that of the background scenario, should guarantee a low dispersion of the phase values. For high SCR values, the relationship between SCR, phase noise (σ_ϕ), and the dispersion of the displacement measurements along the satellite LOS (σ_{LOS}) can be approximated as follows [4]:

$$\sigma_{\mathrm{LOS}} = \frac{\lambda}{4 \cdot \pi} \cdot \sigma_\phi \approx \frac{\lambda}{4 \cdot \pi} \cdot \sqrt{\frac{1}{2 \cdot \mathrm{SCR}}}. \tag{1}$$

A design requirement on the SCR of 100 (i.e., 20 dB) then corresponds to a dispersion of the displacement measurements in LOS direction of about 0.3 mm at C-band. Since the area available for the experiment was an urban area in Milano (Italy), high SCR values can be achieved only with RCS values of several thousand square meters.

Apart from the SCR, the other major requirement of the experiment concerns the multiplatform visibility. Table I summarizes the main features of the most common reflectors used in radar experiments, namely, flat plate, dihedral [11]–[14], square, and triangular trihedral. Flat plates cannot be used for the experiment since they are visible for one satellite sensor only (either Envisat or Radarsat). In fact, the two radar systems, although both operating at C-band and quite similar for bandwidth and pulse repetition frequency, are characterized by very different Doppler centroid (Dc) values, corresponding to different antenna squint angles (Appendix), at least at midlatitudes. Due to the different Dc values of the target in the two radar systems (no yaw-steering correction is available in Radarsat), by properly pointing a flat reflector with a physical dimension of 1 m^2 for Envisat acquisitions, its RCS in Radarsat images would experience a loss of about 17 dB with respect to the nominal value reported in Table I, making it impossible to have a high SCR in an urban environment.

By comparing the maximum theoretical RCS with the corresponding overall dimensions of the reflectors, it was decided to use a set of dihedral reflectors properly pointed toward both satellite platforms, as discussed in Section IV.

Even if dihedral provides an excellent radar target for the purpose of polarimetric calibration [15]–[17], its application in the InSAR experiment is not so common. Indeed, corner reflectors, having less demanding requirements, are generally deployed. Because of the mechanical stability and the accuracy of the imposed shifts to the reflectors must be better than a fraction of millimeter for this validation exercise, both the size and the weight of the structure to be tracked by the system should be kept limited. As a consequence, the dihedral has been preferred to the more cumbersome structure of the trihedral. Moreover, a by-product of the experiment would have been the validation of the pointing procedure (described in Section IV) based on nominal satellite ephemeredes.

Although not specifically designed for a GPS-InSAR comparison, the experimental setup was completed by two GPS points for differential measurements. The first antenna has been fixed to the mobile platform. Unfortunately, the shape of the basement turned out to be unfavorable to create a measurement point integral with the mobile reflectors, and the GPS antenna could measure only the vertical displacements of the dihedrals. The second antenna was placed 50 m apart from the first one on an area supposed stable. The baseline vector between these two points can then be estimated with high accuracy; in fact, most of the biases affecting the GPS signal are strongly reduced for such a short baseline when processing a double difference carrier phase.

III. DIHEDRAL DESIGN

As already discussed in the previous section, two pairs of dihedral reflectors were designed and manufactured for the experiment: one fixed and one "mobile." The latter was sequentially displaced by an operator both in the horizontal and vertical directions.

The mobile reflectors' assembly [Fig. 1(a)] is made by two metallic frames (manufactured by means of 45×45 and 45×90 mm^2 square/rectangular section standard section aluminum bars). The lower frame, which is robust enough to support the whole reflector structure, is steady and equipped with

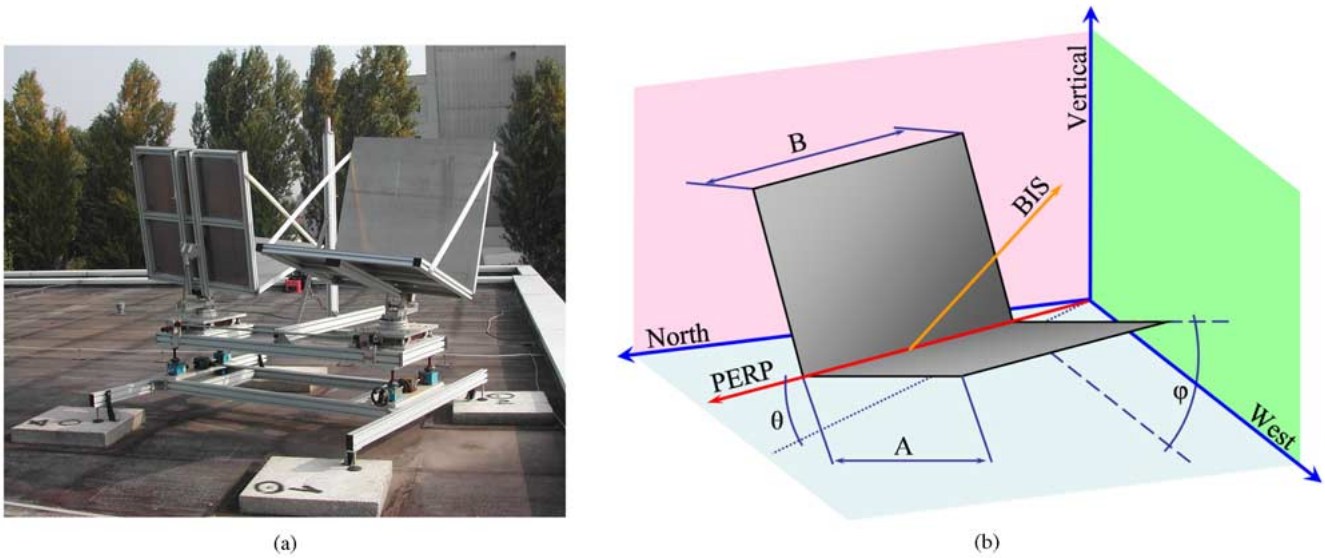

Fig. 1. (a) Mobile reflectors assembly and (b) schematic of a dihedral reflector.

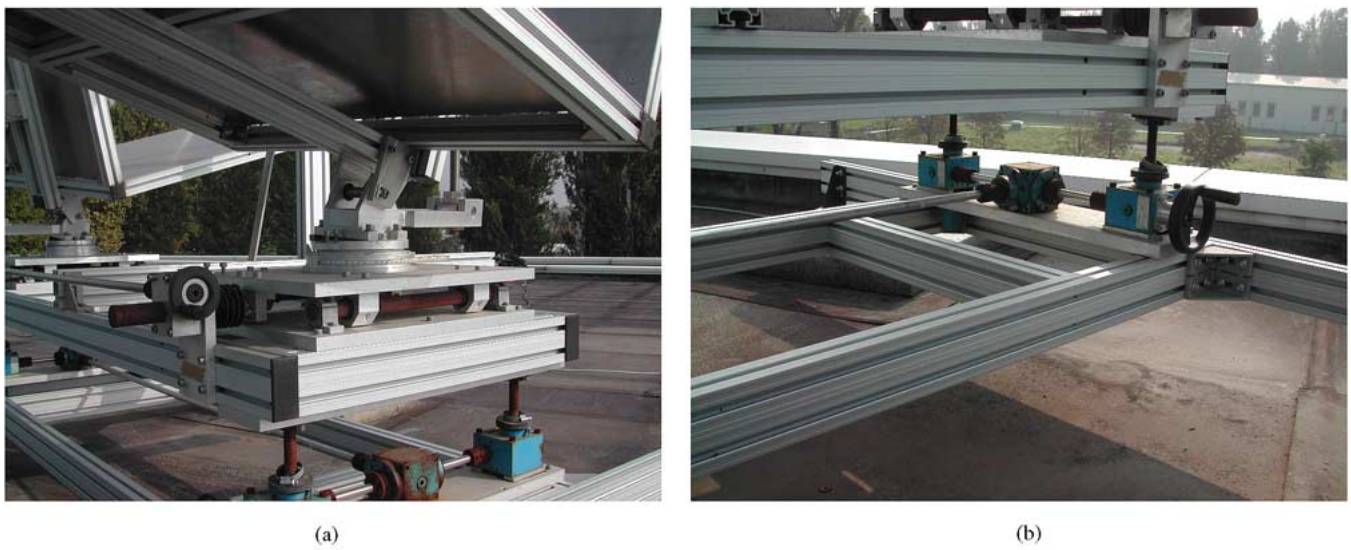

Fig. 2. Mobile reflectors' assembly. The (a) vertical and (b) horizontal translation mechanism.

four protrusive legs (to increase the stability) provided with fastening holes for ground fixation. The upper frame is the mobile one. Vertical displacements of this frame can be generated by means of four screw jacks (50-mm travel range; 0.1-mm screw pitch) positioned between the two frames. To get a uniform vertical displacement, the four jacks are simultaneously driven (via connecting bars) by acting on a unique driving crank [Fig. 2(a)]. Bolted to the upper frame, there are two linear translation units utilized for the horizontal displacements [Fig. 2(b)]. The precise in-plane translation of a mobile platform is provided in each unit by four ball screw assemblies driven by means of screw jacks similar to the previously described ones (50-mm travel range; 0.2-mm screw pitch). As for the vertical translation mechanism, the two jacks are simultaneously driven by means of a unique crank.

The dihedral reflectors are mounted upon the two sliding platforms by means of a robust clamping system. Each reflector is made by two square aluminum plates (1×1 m wide; 2 mm thick), orthogonally mounted on a rigid supporting frame (made by 45×45 mm^2 standard section aluminum bars). The maximum RCS is then 7.845 m^2 at 5.3 GHz. The clamping mechanism has been designed so that rotations of the reflectors around both the vertical and horizontal axes can be performed accurately during the preliminary alignment phase.

By means of multiple measurements carried out on the mobile platform, it was estimated that the mechanical errors (taking into account also the thermal dilation effects) were about 0.3 mm. This high accuracy value is required in order to allow a submillimeter comparison with the InSAR data.

The steady reflectors' assembly is quite similar to the mobile one, but with a simpler mechanical structure. It is, in fact, composed of a single supporting frame where a couple of dihedral reflectors (identical to those utilized in the mobile unit) is rigidly clamped. Apart from the reflector's clamping

mechanism (used to properly point the device), no other moving parts are present in the structure.

IV. Dihedral Deployment

The deployment procedure mainly consists of two steps: 1) identification of the proper locations for the artificial reflectors; and 2) pointing of the dihedrals.

The selection of the best site is carried out by taking into account the three basic requirements.

1) The reflectors should be installed in a protected area under control of the validation team for the whole duration of the campaign (almost one year).
2) The SCR should be high enough in all acquisitions so that the theoretical precision of LOS displacement measurements would be better than 1 mm.
3) The reflectors should be not too far apart, so that the impact of atmospheric effects can be considered negligible.

Radar amplitude images acquired before the deployment of the artificial reflectors can be used successfully to select suitable areas for the experiment. According to logistic constraints, as explained in [8], the area selected for the experiment was a flat roof of a building. The two stations are about 50 m apart, making the impact of the atmospheric effects on the phase values extremely weak [18]. Indeed, one of the most significant error terms affecting the InSAR measurements is due to the so-called "atmospheric phase screen." Having deployed the reflectors very close to each other, this phase disturbance was almost canceled when performing the double phase difference (as explained in Section V).

It was realized, however, that the best configuration could not meet all the requirements on σ_{LOS}, since one of the four reflectors would experience unfavorable SCR values for one acquisition geometry, at least based on the clutter power estimated from the available radar images. Real data analysis partially confirmed this fact, as it will be discussed in Section V.

After the selection of the best areas for the deployment of the reflectors, each dihedral is properly orientated in order to maximize its RCS in all acquisition geometries. As well known, the RCS decreases if the LOS of the radar sensor is not along the symmetry axis of the reflector [11]. Dihedral reflectors are then very sensitive to pointing errors in the azimuth direction.

Since each reflector should be visible in both Envisat and Radarsat acquisitions, an *ad hoc* deployment procedure has to be adopted. In detail, the following steps are required.

1) For each dihedral, the direction of "maximum illumination" for each radar sensor is computed, i.e., we evaluate the relative position of the satellite with respect to the reflector when the radar illuminates the target with maximum power.
2) Let $\mathbf{L_{rsat}}$ and $\mathbf{L_{envi}}$ be the maximum illumination unit vector of the reflector for Radarsat and Envisat, respectively; $\mathbf{L_{rsat}}$ and $\mathbf{L_{envi}}$ depend on the effective squint angles of the radar antenna estimated from the nominal Dc values (Appendix).
3) Compute the vector cross product: $\mathbf{PERP} = \mathbf{L_{rsat}} \times \mathbf{L_{envi}}$.

TABLE II
Dataset Radarsat Ascending (Standard Beam S3)

#	ACQUISITION	SATELLITE	Dc [Hz]	Bn [m]	Bt [day]
1	24/03/2003	RADARSAT-1	-6253	-172,4	-480
2	17/04/2003	RADARSAT-1	-6331	-100,6	-456
3	11/05/2003	RADARSAT-1	-6546	-437,9	-432
4	04/06/2003	RADARSAT-1	-6206	564,7	-408
5	28/06/2003	RADARSAT-1	-6656	-37,1	-384
6	22/07/2003	RADARSAT-1	-6463	-46,7	-360
7	15/08/2003	RADARSAT-1	-6473	122,0	-336
8	08/09/2003	RADARSAT-1	-6450	459,6	-312
9	02/10/2003	RADARSAT-1	-6428	-261,9	-288
10	26/10/2003	RADARSAT-1	-6556	-239,6	-264
11	19/11/2003	RADARSAT-1	-6449	-626,8	-240
12	22/06/2004	RADARSAT-1	-6756	-90,8	-24
13 (M)	16/07/2004	RADARSAT-1	-6421	0,0	0
14	20/10/2004	RADARSAT-1	-6331	-400,0	96
15	13/11/2004	RADARSAT-1	-6517	77,5	120
16	07/12/2004	RADARSAT-1	-6447	-238,3	144
17	31/12/2004	RADARSAT-1	-6162	-526,1	168
18	24/01/2005	RADARSAT-1	-6279	411,0	192
19	17/02/2005	RADARSAT-1	-6128	-491,7	216
20	13/03/2005	RADARSAT-1	-6471	-218,3	240
21	06/04/2005	RADARSAT-1	-6405	563,9	264
22	30/04/2005	RADARSAT-1	-6455	-556,7	288
23	24/05/2005	RADARSAT-1	-6388	466,0	312
24	17/06/2005	RADARSAT-1	-6715	-547,9	336
25	04/08/2005	RADARSAT-1	-6632	-539,8	384

4) Align the dihedral backbone along the $\mathbf{PERP}$ direction.
5) Rotate the reflector around $\mathbf{PERP}$ so that it points (i.e., it exhibits maximum RCS) toward the direction defined by the bisector vector $\mathbf{BIS}$ of the two radar illumination directions: $\mathbf{BIS} = \mathbf{L_{rsat}} + \mathbf{L_{envi}}$ [as shown in Fig. 1(b)].

From an operational point of view, taking into account the whole pointing procedure and the instruments used, it was estimated that pointing errors were lower than 0.5° corresponding to a loss of less than 1200 m^2 in RCS with respect to the nominal (maximum) value, namely, 7.845 m^2. Of course, any variation in the Dc with respect to the nominal value impacts on the RCS exhibited by the reflector. While this factor is almost negligible in Envisat acquisitions (Dc values are very low and almost identical), for Radarsat, a further loss of 100 m^2 maximum in RCS should be taken into account (Appendix).

V. Experimental Results

The processing was performed using four different datasets acquired over Milano from October 2004 to July 2005: ascending Radarsat Standard Beam S3 (Table II), descending Radarsat Standard Beam S3 (Table III), ascending Envisat Image Mode S2 (Table IV), and descending Envisat Image Mode S2 (Table V).

The experiment was "blind," i.e., the processing team was not aware of the actual displacements affecting the mobile target. However, the maximum differential shift, in both horizontal and vertical directions, was carefully selected so that no phase unwrapping error should be expected in the time series of range variations in any InSAR dataset.

TABLE III
DATASET RADARSAT DESCENDING (STANDARD BEAM S3)

#	ACQUISITION	SATELLITE	Dc [Hz]	Bn [m]	Bt [day]
1	28/04/2003	RADARSAT-1	7134	-530,7	-144
2	22/05/2003	RADARSAT-1	7229	418,1	-120
3	15/06/2003	RADARSAT-1	7269	634,4	-96
4	09/07/2003	RADARSAT-1	7344	-479,5	-72
5	02/08/2003	RADARSAT-1	7247	305,9	-48
6	26/08/2003	RADARSAT-1	7188	453,0	-24
7 (M)	19/09/2003	RADARSAT-1	7151	0,0	0
8	13/10/2003	RADARSAT-1	6983	-298,8	24
9	06/11/2003	RADARSAT-1	6997	-434,5	48
10	30/11/2003	RADARSAT-1	6999	274,2	72
11	24/12/2003	RADARSAT-1	6568	682,8	96
12	17/01/2004	RADARSAT-1	7226	-63,4	120
13	10/02/2004	RADARSAT-1	7131	210,3	144
14	22/04/2004	RADARSAT-1	7141	-508,6	216
15	27/07/2004	RADARSAT-1	7368	122,5	312
16	20/08/2004	RADARSAT-1	7280	25,0	336
17	13/09/2004	RADARSAT-1	7195	117,7	360
18	07/10/2004	RADARSAT-1	7157	-564,6	384
19	24/11/2004	RADARSAT-1	6991	644,2	432
20	18/12/2004	RADARSAT-1	6917	-706,3	456
21	11/01/2005	RADARSAT-1	6846	777,0	480
22	04/02/2005	RADARSAT-1	6737	35,9	504
23	28/02/2005	RADARSAT-1	6817	-406,6	528
24	24/03/2005	RADARSAT-1	7065	175,0	552
25	17/04/2005	RADARSAT-1	7181	29,4	576
26	11/05/2005	RADARSAT-1	7311	119,9	600
27	04/06/2005	RADARSAT-1	7364	690,3	624
28	28/06/2005	RADARSAT-1	7405	225,1	648
29	22/07/2005	RADARSAT-1	7322	706,3	672
30	15/08/2005	RADARSAT-1	7352	-115,9	696

TABLE IV
DATASET ENVISAT ASCENDING (TRACK 487—FRAME 909)

#	ACQUISITION	SATELLITE	Dc [Hz]	Bn [m]	Bt [day]
1	06/07/2003	ENVISAT	80	-54,5	-245
2	10/08/2003	ENVISAT	18	137,8	-210
3	19/10/2003	ENVISAT	-50	279,1	-140
4 (M)	07/03/2004	ENVISAT	0	0,0	0
5	11/04/2004	ENVISAT	-6	352,7	35
6	16/05/2004	ENVISAT	-1	-192,2	70
7	20/06/2004	ENVISAT	-5	50,9	105
8	16/01/2005	ENVISAT	1	-398,2	315
9	27/03/2005	ENVISAT	-6	-99,8	385
10	10/07/2005	ENVISAT	-8	-297,9	490

Each dataset was processed independently. First, all images have been oversampled both in range and azimuth directions, and coregistered with respect to a reference image or master. Then, the differential interferograms have been generated, as well as the time series of the amplitude returns. Finally, the LOS displacement time series has been extracted, and the EW and vertical components have been estimated.

A. Amplitude Analysis

As already mentioned in the previous section, the time series analysis of the amplitude values of the image pixels corresponding to the locations of the reflectors allows an estimation of the SCR value, assuming stationary clutter conditions. Operationally, the clutter power can be computed as the mean of the intensity values corresponding to those images (at least seven images for all datasets) acquired before the deployment of the dihedrals, whereas the other samples are used to extract the mean reflector backscattered signal.

TABLE V
DATASET ENVISAT DESCENDING (TRACK 208—FRAME 2691)

#	ACQUISITION	SATELLITE	Dc [Hz]	Bn [m]	Bt [day]
1	02/07/2002	ENVISAT	-39	-20,2	-280
2	06/08/2002	ENVISAT	-134	-644,1	-245
3	15/10/2002	ENVISAT	-97	-490,9	-175
4	04/03/2003	ENVISAT	-126	-993,2	-35
5 (M)	08/04/2003	ENVISAT	0	0,0	0
6	13/05/2003	ENVISAT	11	120,3	35
7	17/06/2003	ENVISAT	-27	-300,0	70
8	30/09/2003	ENVISAT	-182	-297,0	175
9	04/11/2003	ENVISAT	-155	-1004,5	210
10	17/02/2004	ENVISAT	-91	-648,1	315
11	23/03/2004	ENVISAT	-84	844,6	350
12	01/06/2004	ENVISAT	-85	244,3	420
13	06/07/2004	ENVISAT	-87	-389,0	455
14	23/11/2004	ENVISAT	-87	-81,4	595
15	12/04/2005	ENVISAT	-86	-41,2	735
16	17/05/2005	ENVISAT	-88	69,7	770
17	21/06/2005	ENVISAT	-89	222,2	805
18	26/07/2005	ENVISAT	-88	329,6	840

TABLE VI
ESTIMATED DISPERSION OF LOS DISPLACEMENT FROM SCR ASI VALUES

#	REFERENCE DIHEDRAL	MOBILE DIHEDRAL
RADARSAT (Ascending orbits)	SCR=5.65 dB → σ_{LOS} = 1.66 mm ASI= 10.33 → σ_{LOS} = 0.44 mm	SCR=11.1 dB → σ_{LOS} = 0.89 mm ASI= 8.09 → σ_{LOS} = 0.56 mm
RADARSAT (Descending orbits)	SCR=12.8 dB → σ_{LOS} = 0.73 mm ASI= 17.15 → σ_{LOS} = 0.26 mm	SCR=13.1 dB → σ_{LOS} = 0.70 mm ASI= 14.12 → σ_{LOS} = 0.32 mm
ENVISAT (Ascending orbits)	SCR=14.7 dB → σ_{LOS} = 0.59 mm	SCR=14.6 dB → σ_{LOS} = 0.59 mm
ENVISAT (Descending orbits)	SCR=15.7 dB → σ_{LOS} = 0.52 mm	SCR=18.7 dB → σ_{LOS} = 0.37 mm

Table VI summarizes the estimated SCR values for the reference and mobile dihedrals for all acquisition geometries. Three out of four reflectors exhibit an estimated SCR value higher than 10 dB, allowing precise $(\sigma_{\mathrm{LOS}} < 1$ mm$)$ displacement estimates (1), at least theoretically. One is characterized by a rather poor SCR (< 6 dB), as was already foreseen during the design phase of the experiment.

Apart from the ratio of the signal intensity before and after the deployment of the reflector, the expected phase noise can be estimated by computing the dispersion index of the amplitude values relative to the time series of each reflector. The amplitude stability index (ASI) is a simple statistical parameter already used successfully in the PS technique for the identification of the so-called "PS candidates," and it is defined as the ratio of the mean (m_{A}) and the standard deviation (σ_{A}) of the amplitude data returns [2].

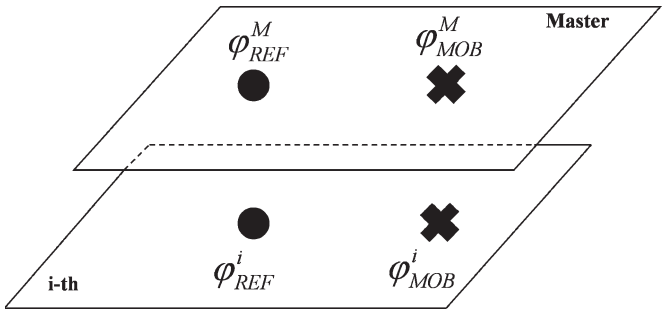

Fig. 3. LOS displacement estimation using differential phase observations at the reflector locations.

The difference between the SCR and the ASI values is related to the methodology adopted to estimate the noise level. In the former, the clutter power is estimated by using the radar images acquired before the experiment (with no reflector) and by supposing a certain RCS for the artificial reflector to be installed. In other words, the estimated SCR value assumes that the superposition of the effects holds and the installation of the artificial reflector will not produce any interaction or shadowing effect with the background clutter of the resolution cell where it will be deployed. Thus, the computed SCR is an "expected SCR."

On the contrary, the ASI value is a measurement of the actual SCR (better to say, the SNR: taking into account both the clutter and the noise level of both the sensor and the processing). The ASI value, of course, could be estimated only after the reflector deployment and after the acquisition of some SAR data. The higher the number of data available, the better the accuracy of the estimation.

For high SNR [2], the following relation holds:

$$\sigma_{\mathrm{LOS}} = \frac{\lambda}{4\cdot\pi}\cdot\sigma_{\phi} \approx \frac{\lambda}{4\cdot\pi}\cdot\frac{1}{\mathrm{ASI}} = \frac{\lambda}{4\cdot\pi}\cdot\frac{\sigma_{\mathrm{A}}}{m_{\mathrm{A}}}. \qquad (2)$$

In Table VI, the ASI values of the four reflectors as well as the estimated dispersion of the LOS displacement measurements are reported for Radarsat acquisitions. In fact, the number of Envisat data available after the installation of the reflectors was not enough to get a reasonable estimation of the ASI values.

It should be noted that, in general, both approaches for the estimation of the phase dispersion based on the amplitude data give a worse SNR for images acquired by Radarsat along ascending orbits. However, the ASI is higher than expected, at least based on the analysis of the images after the deployment of the reflectors.

As a matter of fact, the precision of the InSAR measurements turned out to be comparable with the accuracy expected from the ASI values, taking into account the contribution expected from unavoidable *in situ* mechanical effects and spurious atmospheric components, as well as processing artifacts, as it will be discussed in Section VI.

B. LOS Measurements

As shown in Fig. 3, the LOS displacement corresponding to the ith acquisition is computed through a phase difference between the reference reflector (suffix REF) and the mobile one (suffix MOB):

$$\Delta\varphi^{i} = \left(\varphi^{i}_{\mathrm{MOB}} - \varphi^{i}_{\mathrm{REF}}\right) - \left(\varphi^{M}_{\mathrm{MOB}} - \varphi^{M}_{\mathrm{REF}}\right) \qquad (3)$$

where the superscript M indicates the master acquisition (i.e., the temporal reference) and i is the slave image under study.

Since the position of the reflectors was known with submeter accuracy, owing to the GPS measurements carried out at the beginning of the experiment, all phase components related to the positions of the radar targets were easily compensated for, allowing a rather straightforward extraction of the motion components. In fact, owing to the closest distance (e.g., about 50 m) separating the reflectors and the spatial behavior (e.g., low pass) of the tropospheric and ionospheric phase components, the impact of the atmospheric effects could be reasonably neglected by the double phase difference.

Figs. 4 and 5 show the retrieved LOS displacements for Radarsat and Envisat data (ascending and descending orbits), as well as the ground truth data obtained from the horizontal and vertical displacement values imposed on the mobile station by the validation team, projected into the satellite LOS. Maximum errors and standard deviation values are reported in Tables VII–X.

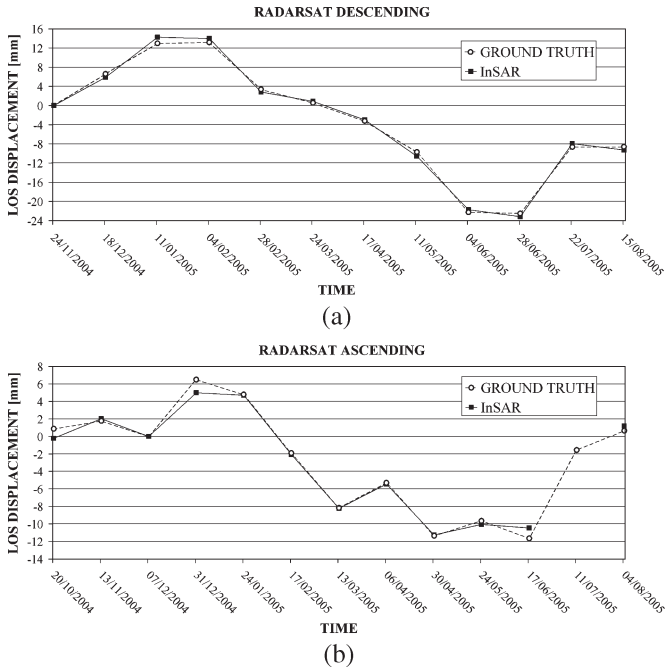

Fig. 4. LOS displacements retrieved by Radarsat data in comparison with the projection of the true values components along the corresponding radar sight. (a) Descending data. (b) Ascending data.

C. Estimation of Horizontal and Vertical Components

In order to properly combine the LOS estimations derived from different acquisition geometries at different times, we referred to the known scheduled shifts of the reflectors, as shown in Table XI. The ascending and descending LOS measurements

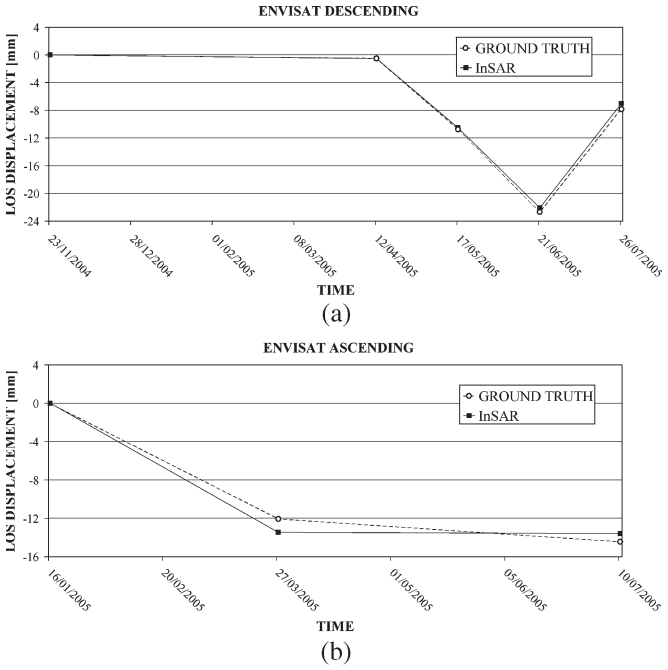

Fig. 5. LOS displacements retrieved by Envisat data in comparison with the projection of the true values components along the corresponding radar sight. (a) Descending data. (b) Ascending data.

TABLE VII
LOS DISPLACEMENTS RETRIEVED BY RADARSAT ASCENDING DATA IN COMPARISON WITH THE PROJECTION OF THE TRUE VALUES OF THE DISPLACEMENT COMPONENTS ALONG THE CORRESPONDING RADAR LOS

DATE	RADARSAT ASCENDING LOS [mm]	GROUND TRUTH [mm]			ERROR [mm]	STD [mm]
		E-W	U-D	LOS		
20/10/2004	-0.22	-8.00	-4.72	0.85	1.07	0.69
13/11/2004	2.02	-3.02	0.00	1.76	-0.26	
07/12/2004	0.00	0.00	0.00	0.00	0.00	
31/12/2004	4.99	0.00	8.04	6.50	1.51	
24/01/2005	4.70	7.00	10.95	4.77	0.07	
17/02/2005	-2.08	13.02	6.99	-1.94	0.14	
13/03/2005	-8.24	10.04	-2.89	-8.19	0.05	
06/04/2005	-5.45	5.10	-2.89	-5.31	0.14	
30/04/2005	-11.27	7.11	-8.95	-11.38	-0.11	
24/05/2005	-10.07	0.01	-11.9	-9.63	0.44	
17/06/2005	-10.46	-9.03	-20.92	-11.65	-1.19	
04/08/2005	1.18	-8.03	-4.99	0.65	-0.53	

TABLE VIII
LOS DISPLACEMENTS RETRIEVED BY RADARSAT DESCENDING DATA IN COMPARISON WITH THE PROJECTION OF THE TRUE VALUES OF THE DISPLACEMENT COMPONENTS ALONG THE CORRESPONDING RADAR LOS

DATE	RADARSAT DESCENDING LOS [mm]	GROUND TRUTH [mm]			ERROR [mm]	STD [mm]
		E-W	U-D	LOS		
24/11/2004	0.00	0.00	0.00	0.00	0.00	0.72
18/12/2004	5.86	0.00	8.04	6.58	0.72	
11/1/2005	14.25	7.00	10.95	12.95	-1.30	
4/2/2005	13.97	13.02	6.99	13.14	-0.83	
28/2/2005	2.80	10.04	-2.89	3.36	0.56	
24/3/2005	0.85	5.10	-2.89	0.54	-0.31	
17/4/2005	-2.99	7.11	-8.95	-3.27	-0.27	
11/5/2005	-10.57	0.01	-11.9	-9.73	0.84	
4/6/2005	-21.72	-9.03	-20.92	-22.26	-0.54	
28/6/2005	-23.19	-18.03	-14.92	-22.49	0.70	
22/7/2005	-7.93	-8.03	-4.99	-8.66	-0.73	
15/08/2005	-9.27	-8.03	-4.99	-8.66	0.61	

TABLE IX
LOS DISPLACEMENTS RETRIEVED BY ENVISAT ASCENDING DATA IN COMPARISON WITH THE PROJECTION OF THE TRUE VALUES OF THE DISPLACEMENT COMPONENTS ALONG THE CORRESPONDING RADAR LOS

DATE	ENVISAT ASCENDING LOS [mm]	GROUND TRUTH [mm]			ERROR [mm]	STD [mm]
		E-W	U-D	LOS		
16/01/2005	0.00	0.00	0.00	0.00	0.00	1.14
27/03/2005	-13.46	-1.90	-13.84	-12.05	1.40	
10/07/2005	-13.60	-25.03	-25.87	-14.45	-0.85	

TABLE X
LOS DISPLACEMENTS RETRIEVED BY ENVISAT DESCENDING DATA IN COMPARISON WITH THE PROJECTION OF THE TRUE VALUES OF THE DISPLACEMENT COMPONENTS ALONG THE CORRESPONDING RADAR LOS

DATE	ENVISAT DESCENDING LOS [mm]	GROUND TRUTH [mm]			ERROR [mm]	STD [mm]
		E-W	U-D	LOS		
23/11/2004	0.00	0.00	0.00	0.00	0.00	0.38
12/04/2005	-0.53	5.10	-2.89	-0.51	0.02	
17/05/2005	-10.53	0.01	-11.9	-10.78	-0.25	
21/06/2005	-22.09	-9.03	-20.92	-22.69	-0.60	
26/07/2005	-7.01	-8.03	-4.99	-7.84	-0.83	

TABLE XI
SCHEDULED MOVEMENTS AND SAR IMAGES ACQUIRED DURING THE EXPERIMENT

DATE OF MOVEMENT	RADARSAT ASCENDING	RADARSAT DESCENDING	ENVISAT ASCENDING	ENVISAT DESCENDING
23/11/2004	07/12/2004	24/11/2004	Not acquired	23/11/2004
15/12/2004	31/12/2004	18/12/2004	Not acquired	Not acquired
10/01/2005	24/01/2005	11/01/2005	16/01/2005	Not acquired
02/02/2005	17/02/2005	04/02/2005	Not acquired	Not acquired
24/02/2005	13/03/2005	28/02/2005	Not acquired	Not acquired
16/03/2005	06/04/2005	24/03/2005	27/03/2005	12/04/2005
13/04/2005	30/04/2005	17/04/2005	Not acquired	Not acquired
06/05/2005	24/05/2005	11/05/2005	Not acquired	17/05/2005
01/06/2005	17/06/2005	04/06/2005	10/07/2005	21/06/2005
20/07/2005	04/08/2005	22/07/2005	Not acquired	26/07/2005

can be related to the components of the displacement vector according to the following equations:

$$\begin{bmatrix} \nu_{\mathrm{ASCE}} \\ \nu_{\mathrm{DESCE}} \end{bmatrix} = \begin{bmatrix} a_{\mathrm{UD}}^{\mathrm{ASCE}} & a_{\mathrm{EW}}^{\mathrm{ASCE}} \\ a_{\mathrm{UD}}^{\mathrm{DESCE}} & a_{\mathrm{EW}}^{\mathrm{DESCE}} \end{bmatrix} \begin{bmatrix} x_{\mathrm{UD}} \\ x_{\mathrm{EW}} \end{bmatrix}$$
$$\mathbf{v} = \mathbf{A} \cdot \mathbf{x} \tag{4}$$

where $\mathbf{v}$ is the vector of the estimated displacements along the two LOSs, $\mathbf{A}$ is the matrix of the up–down (UD) and EW components of the sensitivity vectors (i.e., the unit vectors related to the satellite LOS), and $\mathbf{x}$ is the unknown components of the displacement vector. Equations in (4) are derived supposing that the north–south component is null, as discussed in the Introduction. Since the matrix $\mathbf{A}$ is nonsingular, the exact analytical solution can be easily computed.

Unfortunately, the low number of Envisat scenes acquired during the experiment (due to conflicts in the acquisition planning over the test area) did not allow us to apply a multiplatform approach, where Envisat and Radarsat data are jointly used to recover the displacement vector. As a consequence, the estimation of the horizontal and vertical components of the displacement vector has been performed using the Radarsat data only.

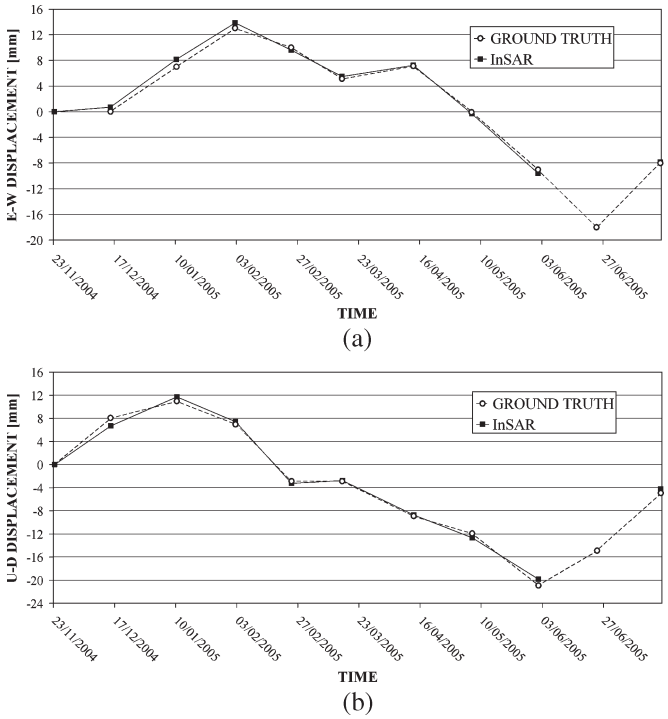

Fig. 6. Comparison between the DInSAR displacement time series and the ground truth data. A blue triangle corresponds to a DInSAR displacement and a purple square to a ground truth data. (a) EW displacement component. (b) UD displacement component.

TABLE XII
DISPLACEMENTS RETRIEVED BY COMBINING RADARSAT ASCENDING AND DESCENDING DATA IN COMPARISON WITH GROUND TRUTH VALUES

DATE	InSAR [mm]		GROUND TRUTH [mm]		ERROR [mm]		STD [mm]	
	E-W	U-D	E-W	U-D	E-W	U-D	E-W	U-D
23/11/2004	0.00	0.00	0.00	0.00	0.00	0.00	0.58	0.75
15/12/2004	0.70	6.68	0.00	8.04	-0.70	1.36		
10/01/2005	8.18	11.72	7.00	10.95	-1.18	-0.77		
02/02/2005	13.86	7.42	13.02	6.99	-0.84	-0.43		
24/02/2005	9.60	-3.27	10.04	-2.89	0.44	0.38		
16/03/2005	5.49	-2.79	5.10	-2.89	-0.39	-0.10		
13/04/2005	7.25	-8.71	7.11	-8.95	-0.14	-0.24		
06/05/2005	-0.33	-12.69	0.01	-11.90	0.34	0.79		
01/06/2005	-9.60	-19.86	-9.03	-20.92	0.57	-1.06		
19/07/2005	-7.87	-4.21	-8.03	-4.99	-0.16	-0.78		

In Fig. 6, the time series of the horizontal and vertical components estimated from the Radarsat dataset is reported. The standard deviation of the estimated displacements is 0.75 and 0.58 mm for vertical and horizontal components, respectively (Table XII). These numbers are the most important achievement of this project. They show that under favorable conditions and high SNR, submillimetric precision of the estimated displacement values can be achieved using satellite radar observation.

D. GPS Data Analysis

GPS data were collected at the beginning and at the end of the temporal window of SAR acquisitions, i.e., from October 2004 to July 2005. These data have been observed over sessions lasting, in most of the cases, more than 24 h. Data processing has been based on computing the double difference carrier phase using the Bernese 5.0 scientific software [19], which allows for the highest quality standard.

TABLE XIII
DISPLACEMENTS RETRIEVED BY GPS DATA IN COMPARISON WITH THE GROUND TRUTH VALUES

DATE	GPS DATA [mm]		GROUND TRUTH [mm]	ERROR [mm]
	U-D	STD	U-D	U-D
26/10/2004	3.45	0.8	4.72	1.27
23/11/2004	4.46	0.8	4.72	0.26
15/12/2004	9.97	4.7	12.76	2.79
13/04/2005	-2.31	1.3	-4.23	-1.92
01/06/2005	-15.14	2.7	-16.2	-1.06
24/06/2005	-14.82	1.7	-16.2	-1.37
19/07/2005	-7.07	1.9	-10.2	-3.13

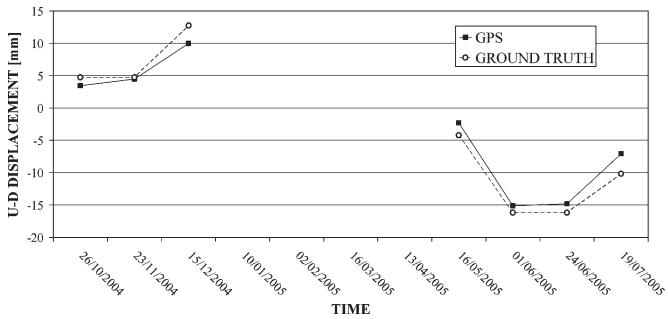

Fig. 7. GPS displacement estimations compared with ground truth data. (UD direction).

The quasi-iono free strategy for ambiguity fixing has been adopted, and CODE ionospheric parameters have been considered to reduce the ionospheric perturbation in L1 and L2 carrier phase observables. The tropospheric zenith path delay has been modeled by the Dry-Neill model, estimating one hourly parameter in the Wet-Neill mapping function. Horizontal gradient parameters have also been estimated. The coordinates have been computed using the iono-free observable, weighting the observations with the elevation-dependent function $\cos^2(z)$ (z is the satellite zenith angle).

The coordinates of the two points have been estimated in the IGb00 reference frame [20] by using three IGS permanent stations (WTZR, GRAZ, ZIMM) and precise IGS ephemerides.

Then, (N, E, U) coordinates were computed with respect to a local cartesian reference frame having its origin in point B (i.e., the "reference antenna"). The local coordinate variations have been referred to the estimates of October 18th, which is hence our starting position. The estimated GPS variations are listed in Table XIII.

As already mentioned, the position of the GPS antenna was such that only the vertical displacements of the reflectors could be recorded and compared with ground truth. Indeed, the GPS estimates, as reported in Fig. 7, are close to the experimental variations. A t-Student test (at the significance level $\alpha = 5\%$) proves that these estimates are statistically coherent with those imposed during the experiment.

VI. Discussion

As stated in (3), LOS displacements are evaluated by a phase difference. Thus, assuming the uncorrelated noise components, it follows that

$$\sigma^2_{\Delta\varphi^i} = \left(\sigma^2_{\mathrm{MOB},i} + \sigma^2_{\mathrm{REF},i}\right) + \left(\sigma^2_{\mathrm{MOB},M} + \sigma^2_{\mathrm{REF},M}\right). \quad (5)$$

The phase dispersion of each InSAR measurement is then the sum of four contributions: two depend on the ith acquisition, whereas the others are related to the reference image. Due to this fact, each LOS measurement is affected by a systematic error (i.e., a bias) that is caused by the noise superimposed to the master acquisition.

Using (5) and the dispersion of the LOS measurements estimated from the ASI values (Table VI), it is possible to estimate the *a priori* covariance matrix $\mathbf{C_D}$ of the input data:

$$\mathbf{C_D} = \begin{bmatrix} \sigma^2_{\mathrm{LOS,ASCE}} & 0 \\ 0 & \sigma^2_{\mathrm{LOS,DESCE}} \end{bmatrix} = \begin{bmatrix} 0.71^2 & 0 \\ 0 & 0.41^2 \end{bmatrix}. \quad (6)$$

In order to retrieve the expected accuracy of the vertical and EW displacements, we can compute the *a posteriori* covariance matrix $\mathbf{C_M}$. By substituting the Radarsat sensitivity vectors into the $\mathbf{A}$ matrix and taking into account the matrix $\mathbf{C_D}$, it results that

$$\mathbf{C_M} = \left[\mathbf{A^T C_D^{-1} A}\right]^{-1} = \begin{bmatrix} 0.50^2 & -0.15 \\ -0.15 & 0.71^2 \end{bmatrix}. \quad (7)$$

According to (6), the vertical component is resolved better than the EW. In detail, the theoretical standard deviation for the UD direction is 0.50 mm, whereas for the EW component, it is 0.71 mm.

It is interesting to compare the expected values with those computed by the experimental data. According to the experimental results, the standard deviation for the UD component is 0.75 mm, and it is 0.58 mm along the EW direction. Such a high accuracy level for both horizontal and vertical displacements of a time series (not a single measurement) of the InSAR data turns out to be comparable with the accuracy of the mechanical device used for the ground truth (about 0.3 mm as stated in Section III).

GPS data demonstrated that under ideal conditions and using a state-of-the-art software, the GPS can achieve a millimetric accuracy also in the vertical direction.

VII. Conclusion

Compared to other experiments involving artificial reflectors, the experiment reported in this paper presents some new interesting features.

First of all, in order to carry out a validation experiment with submillimeter accuracy, we were somewhat "forced" to use the dihedral reflector. In fact, both the weight and the dimension of the structure to be tracked represent main practical design requirements to guarantee high mechanical stability and accurate positioning systems (e.g., the ground-truth data should be collected with submillimeter accuracy too). Even if the use of dihedral reflector made the experiment more challenging from the technical point of view, the final results show an unprecedented precision.

A new pointing procedure that allows dihedral reflectors to be visible from two different satellite platforms (i.e., Envisat and Radarsat) was developed and successfully tested. It was found that it was possible to accomplish a multiplatform analysis using the same radar target. Unfortunately, the low number of Envisat scenes acquired during the experiment did not allow the completion of this analysis.

Nevertheless, for the first time, the possibility of combining multigeometry (e.g., ascending and descending orbits) SAR acquisitions in order to retrieve a 2-D displacement time series with submillimeter accuracy has been demonstrated. In more detail, the accuracy for the vertical movement results equal to 0.75 mm, whereas for the EW component, it is 0.58 mm. The retrieved U-D dispersion results were slightly lower than the theoretical value, while the E-W component is resolved better than expected.

Such a high accuracy was a consequence of the following.

1) Significant time and resources devoted to the design, the planning, the implementation, the control, and the performance of the experiment.
2) The mobile structure and the mechanism for imposing the displacement were carefully designed, manufactured, assembled, and operated.
3) All *in situ* effects were minimized by properly selecting the site and preventing any natural or anthropogenic interferences.
4) The impact of atmospheric effects was minimized by considering two reflectors less than 50 m apart: this is well below the correlation length of tropospheric and ionospheric components. Indeed, one of the most significant error terms affecting the InSAR measurements is due to the so-called "atmospheric phase screen." Having deployed the reflectors very close to each other, this phase disturbance was almost canceled by the double phase difference.
5) GPS data have been used to properly remove the topographic phase components.
6) SAR data processing has been performed using state-of-the-art software procedures developed internally.

Another interesting result has been derived by the amplitude and the phase analysis of each deployed reflectors: usually, amplitude data are neglected in InSAR validation exercise. It is the first time that both amplitude and phase information gathered during the duration of the experiment exhibit such a good agreement. Moreover, the computed ASI index values provide an extremely powerful cross-check of the reliability of the achieved results.

It should be pointed out that this experiment was just one step toward a full validation of the PS approach using artificial reflectors. In fact, although we have demonstrated that precise displacement measurements can be carried out on radar targets not affected by phase decorrelation phenomena, the procedure

related to the estimation and removal of the atmospheric phase screen superimposed on each radar acquisition was not validated, due to the short distance between the two reflectors. Future research efforts should be devoted to this important topic, although a good agreement between PS and continuous GPS data has already been reported in [21] and [22].

In the future, the combination of GPS and InSAR technology will provide a powerful tool for imaging land deformation. GPS data can provide an absolute calibration for PS data [23], high temporal resolution to detect abrupt changes, high velocity accuracy in three dimensions, and calibration of SAR measurements to remove low-frequency components due to ionospheric effects and orbital fringes. PS interferometry provides a remarkable spatial coverage compared to the GPS, and new SAR sensors will increase significantly the number of SAR images gathered over a certain area. Urban areas are particularly amenable to PSInSAR analysis. The joint combination of both Radarsat and ESA SAR images acquired along both ascending and descending orbits could provide more than 2000 PS/km^2 over most of the cities, making the monitoring of individual buildings feasible. If the density of GPS stations is high enough, the vertical components of the local velocity field can be estimated using single-geometry SAR datasets by removing the contribution of the GPS-derived horizontal velocity field from the InSAR range change rates [24]. For sure, the identification of synergistic strategies for the combination of both GPS and PS data will be the subject of future developments.

APPENDIX

The RCS of a dihedral reflector depends on its dimensions and orientation. Theoretically, the relationship between RCS and these angles can be determined only by using very accurate model for backscattering [13]. Nevertheless, a closed-form formula for the RCS of a perfectly conducting dihedral at arbitrary aspect angles can be found in [11] and [12]. The latter formula is valid for incident angles close to the symmetry axis of the reflector, and it is then applicable to the experiment under study. According to [12], the RCS is proportional to the following function:

$$\text{RCS} \propto \left(\frac{\sin(X)}{X}\right)^2 \tag{A1}$$

where

$$X = \frac{2 \cdot \pi}{\lambda} \cdot L \cdot \cos(\theta) \cdot \sin(\phi) \tag{A2}$$

and L is the dihedrals' edge length.

Because the dihedral orientation was performed using a GPS compass and electronic leveling, the positioning could contain "man-induced" errors. For example, considering a position accuracy of 0.5°, it results from (A2) that the RCS loss for a dihedral with 1×1 m surfaces is 1177 m^2. As is well known, the Dc value of a SAR acquisition affects the direction of the illuminating wave. As a consequence, it is interesting to investigate the effect of this parameter on the RCS of a radar target shaped as a dihedral. The Doppler frequency f_{D} is related to the squint angle $\varphi_{\mathrm{squint}}$ by the relationship

$$f_{\mathrm{D}} = \frac{2 \cdot \nu_{\mathrm{sat}}}{\lambda} \cdot \sin(\varphi_{\mathrm{squint}}) \tag{A3}$$

where ν_{sat} is the velocity of the satellite platform. Considering a Doppler frequency variation Δf_{D} of 600 Hz (the maximum frequency difference exhibited by all the processed scenes is equal to 583 Hz), the pointing error $\Delta\varphi_{\mathrm{squint}}$ with respect to the reference ϕ angle is given by

$$\Delta\varphi_{\mathrm{squint}} = \left|\varphi_{\mathrm{squint}} - \arcsin\left(\frac{\lambda \cdot (f_{\mathrm{D}} + \Delta f_{\mathrm{D}})}{2 \cdot \nu_{\mathrm{sat}}}\right)\right|. \tag{A4}$$

The worst case presents a maximum angle error of 0.14° that corresponds to an RCS loss lower than 100 m^2. To conclude, a limited Doppler frequency variation has a negligible impact on the dihedral RCS value.

Therefore, the main source of RCS loss for dihedral reflectors is represented by orientation errors. Deployment of dihedral reflectors then requires very accurate pointing procedures as well as a good knowledge of the satellite acquisition geometry.

ACKNOWLEDGMENT

The authors would like to thank A. Fumagalli for his support in SAR data processing.

REFERENCES

[1] P. A. Rosen *et al.*, "Synthetic aperture radar interferometry," *Proc. IEEE*, vol. 88, no. 3, pp. 333–382, Mar. 2000.

[2] A. Ferretti, C. Prati, and F. Rocca, "Permanent scatterers in SAR interferometry," *IEEE Trans. Geosci. Remote Sens.*, vol. 39, no. 1, pp. 8–20, Jan. 2001.

[3] C. Prati, F. Rocca, and A. Monti Guarnieri, "SAR interferometry experiments with ERS-1," in *Proc. 1st ERS-1 Symp.—Space Service Our Environment*, Cannes, France, Nov. 4–8, 1992, pp. 211–218. ESA SP-359.

[4] G. Ketelaar, P. Marinkovic, and R. Hanssen, "Validation of point scatterer phase statistics in multi-pass InSAR," in *Proc. CEOS SAR Workshop*, Ulm, Germany, May 27–28, 2004.

[5] P. Marinkovic, G. Ketelaar, and R. Hanssen, "A controlled Envisat/ERS permanent scatterer experiment, implications of corner reflector monitoring," in *Proc. CEOS SAR Workshop*, Ulm, Germany, May 27–28, 2004.

[6] Y. Xia, H. Kaufmann, and X. Guo, "Differential SAR interferometry using corner reflectors," in *Proc. Int. Geosci. and Remote Sens. Symp.*, Toronto, ON, Canada, Jun. 24–28, 2002, pp. 1243–1246.

[7] L. Timmen, Y. Xia, C. Reigber, R. Hartmann, T. Fiksel, W. Winzer, and J. Knoch-Weber, "Monitoring of small motions in mining areas by SAR interferometry," in *Proc. Fringe*, 1996.

[8] G. Savio, A. Ferretti, F. Novali, S. Musazzi, C. Prati, and F. Rocca, "PSInSAR validation by means of a blind experiment using dihedral reflectors," in *Proc. FRINGE Workshop*, 2005. ESA SP-610.

[9] F. Rocca, "3D motion recovery from multiangle and/or left right interferometry," in *Proc. Fringe*, 2003.

[10] S. Sircar, C. Randell, D. Power, J. Youden, and E. Gill, "Measuring 3-D ground movement by differential interferometry: Technique and validation," in *Proc. IEEE NECEC*, St. John's, NF, Canada, 2003.

[11] E. F. Knott, "RCS reduction of dihedral corners," *IEEE Trans. Antennas Propag.*, vol. AP-25, no. 3, pp. 406–409, May 1977.

[12] S.-Y. Wang and S.-K. Lee, "A compact RCS formula for a dihedral corner reflector at arbitrary aspect angles," *IEEE Trans. Antennas Propag.*, vol. 46, no. 7, pp. 1112–1113, Jul. 1998.

[13] K. Hayashi, R. Sato, Y. Yamaguchi, and H. Yamada, "Polarimetric scattering analysis for a finite dihedral corner reflector," *IEICE Trans. Commun.*, vol. E89-B, no. 1, pp. 191–195, Jan. 2006.

[14] P. Corona, A. De Bonitatubus, G. Ferrara, and C. Gennarelli, "A very accurate model for backscattering by right angled dihedral corners," in *Proc. IEEE Antenna and Propag. Soc. Int. Symp.*, May 1990, vol. 4, pp. 1734–1737.
[15] C. J. Bradley, P. J. Collins, J. Fortuny-Guasch, M. L. Hastriter, G. Nesti, A. J. Terzuoli, Jr., and K. S. Wilson, "An investigation of bistatic calibration objects," *IEEE Trans. Geosci. Remote Sens.*, vol. 43, no. 10, pp. 2177–2184, Oct. 2005.
[16] R. Z. Schneider, K. Papathanassiou, I. Hajnsek, and A. Moreira, "Coherent scatterers in urban areas: Characterisation and information extraction," in *Proc. Fringe*, 2005.
[17] M. Satake, T. Umehara, A. Nadai, H. Maeno, S. Uratsuka, T. Matsuoka, and H. Honma, "Development of polarization selective corner reflectors and its experiment for calibration of airborne polarimetric synthetic aperture radar," in *Proc. IGARSS*, 2001, pp. 417–419.
[18] R. Hanssen, *Radar Interferometry: Data Interpretation and Error Analysis*. Norwell, MA: Kluwer, 2001.
[19] U. Hungenobler, R. Dach, and P. Fridez, *Bernese GPS Software*. Berne, Switzerland: Univ. Berne, 2004. Version 5.0.
[20] J. Ray, D. Dong, and Z. Altamimi, "IGS reference frames: Status and future improvements," *GPS Solut.*, vol. 8, no. 4, pp. 251–266, Dec. 2004.
[21] C. Colesanti, A. Ferretti, C. Prati, and F. Rocca, "Monitoring landslides and tectonic motions with the permanent scatterers technique," *Eng. Geol.*, vol. 68, no. 1/2, pp. 3–14, 2003.
[22] A. Ferretti, C. Colesanti, C. Prati, and F. Rocca, "Comparing GPS, optical levelling and permanent scatterers," in *Proc. IGARSS*, Sydney, Australia, Jul. 9–13, 2001, vol. 6, pp. 2622–2624.
[23] T. H. Dixon, F. Amelung, A. Ferretti, F. Novali, F. Rocca, R. Dokkas, G. Sella, S. W. Kim, S. Wdowinski, and D. Whitman, "Subsidence and flooding in New Orleans," *Nature*, vol. 441, no. 7093, pp. 587–588, Jun. 1, 2006.
[24] R. Bürgmann, G. E. Hilley, A. Ferretti, and F. Novali, "Resolving vertical tectonics in the San Francisco Bay Area from permanent scatterer InSAR and GPS analysis," *Geology*, vol. 34, no. 3, pp. 221–224, Mar. 2006.

Alessandro Ferretti (M'03) was born in Milano, Italy, on January 27, 1968. He received the Laurea degree in electrical engineering (*cum laude*) from Politecnico di Milano (POLIMI), Milan, Italy, in 1993, the "Master" degree in information technology (*cum laude*) from CEFRIEL, Milan, where he was working on digital signal processing, and the Ph.D. degree in electrical engineering from POLIMI, in 1997.

In May 1994, he was with the POLIMI radar group working on SAR interferometry and digital elevation model reconstruction. After devoting most of his research efforts on multitemporal SAR data stacks, he developed, together with Prof. Rocca and Prof. Prati, what is now called the "Permanent Scatterer Technique," a technology patented in 1999 that can overcome most of the difficulties encountered in conventional SAR interferometry. In March 2000, he founded, together with Prof. Rocca, Prof. Prati, and Politecnico di Milano, the company "Tele-Rilevamento Europa" (TRE), where he is currently the Managing Director. He has been involved in many projects financed by the European Space Agency and was the promoter, in 2003, of the first interferometric archive of Radarsat data on a national level. His research interest include radar data processing, optimization algorithms, differential interferometry, and use of remote sensing information for civil protection applications.

Giuliano Savio was born in Bozzolo, Italy, on June 16, 1975. He received the Laurea degree in telecommunication engineering from Politecnico di Milano (POLIMI), Milan, Italy, in 2000.

From 2001 to 2002, he was a Researcher with CEFRIEL, Milan, where he worked in the Advanced Mobile and Wireline Transmission System unit. During this period, he was involved in the radio access network optimization procedures for GSM mobile networks. Since July 2002, he has been with Tele-Rilevamento Europa (TRE), Milan, where he is currently working on PSInSAR processing. His main research interests include nonlinear displacement estimation algorithms and artificial radar reflector development.

Riccardo Barzaghi was born in Milano, Italy, on December 14, 1958. He received the Laurea degree in physics from Università degli Studi di Milano, Milano, in 1982, and the Ph.D. degree in geodesy and surveying sciences from Politecnico di Milano (POLIMI), Milano, in 1987.

In 1990, he was with the Department of Geomatic Engineering. In 2001, he was the Italian National Scientific Coordinator of an INGV-GNDT project which aimed at estimating the deformation style and state of stress of the Calabrian Arc area. Since 2003, he has been a Full Professor of geodesy and geomatics at POLIMI. His research interests are mainly in stochastic methods in geodesy for approximating the Earth gravity potential and in GPS for deformation monitoring.

Prof. Barzaghi is a Fellow of the International Association of Geodesy (IAG) and Director of the International Geoid Service, an official IAG Service.

Alessandra Borghi was born in Bologna, Italy, on June 10, 1971. She received the Laurea degree in physics from Università degli Studi di Bologna, Bologna, Italy, in 1995, and the Ph.D. degree in geodesy and surveying sciences from Politecnico di Milano (POLIMI), Milan, Italy, in 1999.

Since 2000, she has been a Fellow in the Department of Geomatic Engineering. Her research interests are mainly in stochastic methods in geodesy for approximating the Earth gravity potential and in GPS for deformation monitoring.

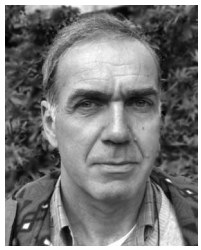

Sergio Musazzi received the degree in physics from the University of Milan, Milan, Italy, in 1978.

He is a Researcher at CESI Ricerca (formerly CISE), Milan. He has worked in different areas of applied optics and remote monitoring techniques. His main research interests in optics include speckle metrology, optical interferometry, light scattering for particle sizing, and spectroscopic techniques. In the field of remote monitoring, his activity has mainly been concerned with the applications of SAR interferometry for landslides monitoring and the stability analysis of industrial structures and with the study of processing techniques for the analysis of high-resolution spaceborne imagery.

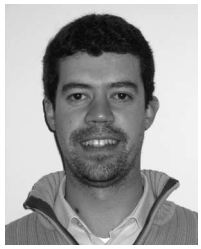

Fabrizio Novali received the Laurea degree (*summa cum laude*) in electronic engineering from Politecnico di Milano (POLIMI), Milan, Italy, in 2000, where he was studying the techniques to estimate and remove atmospheric artifacts in differential SAR interferometry.

He joined Tele-Rilevamento Europa, Milan, working on the permanent scatterers technique and devoting his activity to the development and implementation of algorithms and software. His main research interests are the retrieval of atmospheric phase contributions and of time-nonuniform deformation effects in multi-image SAR interferometry exploiting the PS approach.

Claudio Prati was born in Milan, Italy, on March 20, 1958. He received the Laurea degree in electronic engineering and the Ph.D. degree from the Politecnico di Milano (POLIMI), Milan, in 1983 and 1987, respectively.

He is currently a Full Professor of telecommunications in the Dipartimento di Elettronica ed Informazione, POLIMI. He is a Cofounder of Tele-Rilevamento Europa, which is an RS spin-off company of POLIMI. He has published more than 100 papers on SAR data processing and interferometry. He is the holder of four patents on SAR image processing.

Prof. Prati was the recipient of two prizes from the IEEE Geoscience and Remote Sensing Society (IGARSS'89 and IGARSS'99).

Fabio Rocca received the Dottore in Ingegneria Elettronica in 1962.

He was a Department Chair from 1975 to 1978; a Visiting Professor at Stanford University, Stanford, CA, from 1978 to 1988; and a Commissione d'Ateneo from 1980 to 1993. He is currently a Professor of digital signal processing in the Dipartimento di Elettronica ed Informazione, Politecnico di Milano, Milan, Italy. He is also a Cofounder of two small technological companies, i.e., Telerilevamento Europa and Aresys, which are spin-off companies of Politecnico di Milano. His research includes digital signal processing for television bandwidth compression, emission tomography, seismic data processing, and SAR. He has served in the editorial committees of the *Journal of Seismic Exploration* and *Oil & Gas Science and Technology*.

Prof. Rocca was the President of OGS Trieste from 1982 to 1983 and a Past President of the European Association of Exploration Geophysicists. He was an Honorary Member of the Society of Exploration Geophysicists (SEG) in 1989 and the European Association of Geoscientists and Engineers in 1998. He was the Coordinator of the first EEC research program in geosciences and a member of the Scientific Council of IN-OGS and of the SAR Advisory Group of the European Space Agency. He was the recipient of the HUSPI Award in 1979, the Best Paper Award from IGARSS in 1989 and 1999; the Schlumberger Award in 1990; the Italgas Award for Telecommunications in 1995; the Special SEG Commendation Award in 1998; the Eduard Rhein Foundation Technology Award in 1999; Doctor Honoris Causa in Geophysics from the Institut Polytechnique de Lorraine, Vandoeuvre, France, in 2001; and the Best Paper Award from EUSAR in 2004.